

Hyper-accreting tori of Gamma Ray Bursters

M. V. Barkov

*Department of Applied Mathematics, The University of Leeds, Leeds, LS2 9GT, UK
Space Research Institute, 84/32 Profsoyuznaya Street, Moscow 117997, Russia*

Abstract.

We present numerical simulations of axisymmetric magnetised massive tori around rotating black holes taking into account the energy losses due to emission of neutrinos. A realistic equation of state is used which takes into account the energy losses due to dissociation of nuclei. The heating due to neutrino-antineutrino annihilation is not included. We study the cases of optically thick, semi-transparent, and optically thin to neutrino discs. We show that neutrino cooling does not change significantly the structure of accretion flow and the total energy release. The time scale of accretion is set by the torus angular momentum. Due to the lack of magnetic dynamo in our calculations, it is the initial strength of magnetic field and its topology that determine the process of jet formation and its energetics. Extrapolation of our results gives the total energy released in the jet $\sim 10^{52}$ erg. This is sufficient to explain the hypernovae explosions associated with GRB 980425 and GRB 030329.

Keywords: black hole physics – supernovae: general – gamma-rays: bursts – methods: numerical – MHD – general relativity

PACS: 95.30.Qd; 97.10.Gz; 97.60.Lf; 97.60.Bw

INTRODUCTION

The long-soft Gamma Ray Bursts (GRB) are found predominantly in the blue light of galaxies [1, 2, 3], that is in the region where the most massive stars die. This is supported by the debated connection of GRB 980425 with SN 1998bw [4, 5, 6] and the detection of low-redshift ($z = 0.1685$; [7]) GRB 030329 and its associated supernovae, SN 2003dh [8, 9, 10]. Moreover, the afterglow spectra of many GRBs show broad SN spectral features.

The most popular model of GRB central engine is based on the “failed supernova” scenario of stellar collapse, or “collapsar”, where the iron core of progenitor forms a BH [11]. If the progenitor is non-rotating then its collapse is likely to continue in a “silent” manner until the whole star is swallowed by the BH. If, however, the specific angular momentum in the equatorial part of the stellar envelope exceeds that of the last stable orbit of the BH then the collapse becomes highly anisotropic. While in the polar region it may proceed more or less uninhibited the equatorial layers form dense and massive accretion disk. The gravitational energy released in the disk can be very large, more than sufficient to stop the collapse of outer layers and drive GRB outflows, presumably in the polar direction where the mass density is much lower [12, 13].

The last few years witnessed dramatic progress in general relativistic magnetohydrodynamic (GRMHD) simulations of BH accretion systems. They revealed complex structure that can be decomposed into a disk, corona, disk wind, and highly magnetised polar region that hosts a black hole jet driven by the Blandford-Znajek mechanism [18, 14, 15, 16, 17]. However, all these simulations used very primitive equations of

state (EOS) and neglected neutrino cooling. The first 2D GRMHD simulations in Kerr metrics with realistic EOS and neutrino cooling simulations have been carried out only very recently [19] but the physical time span of their computations was rather short, only $\simeq 0.06$ sec. In this paper we present the results of a similar study whose main aim is to investigate the effects of neutrino cooling processes on the disk structure and dynamics.

PHYSICAL PROCESSES

In these simulations we use realistic EOS [20], which also accounts for the photo-disintegration of nuclei. The cooling rates due to neutrino emission via annihilation of e^+e^- pairs, photo-production, and plasma mechanisms are taken from [21], via URCA processes from [22], and via synchrotron mechanism from [23].

We compare 3 different cases: 1) without cooling (model DL2A9NC); 2) cooling in optically thin regime (model DL2A9C); 3) cooling with incorporated opacity effects (model DL2A9MC). The first case is not very realistic in the GRB context and we consider it only as a reference model. The second case suits well tori with mass of few percent of the solar mass. It could be relevant for the models of neutron star-neutron star and BH-white dwarf mergers. The third case requires a torus of several solar masses.

To describe the neutrino opacity we follow [20], namely we multiply the local loss rate by the factor $e^{-\tau_\nu}$, where $\tau_\nu = S_\nu n l_\nu$ is the neutrino optical depth, $n = \rho/m_p$ is the concentration of baryons, m_p is the proton mass, and S_ν is the neutrino interaction cross-section [24, 25]. Neglecting the pair loading at high densities $S_\nu = ([\kappa_e + \kappa_p]Y_e + \kappa_n(1 - Y_e))T\varepsilon_\nu$, where $\varepsilon_\nu = 3.15kT$, $\kappa_e = \sigma_0\Lambda_e/2m_e^2$, m_e is the electron mass in MeV, $\sigma_0 \simeq 1.71 \times 10^{-44}$ cm², $\Lambda_i = (c_V + c_A)^2 + \frac{1}{3}(c_V - c_A)^2$, where c_V and c_A are the vector and axial-vector coupling constant for given neutrino species. $\Lambda_e \simeq 2.2$, $\kappa_n = \sigma_0(1 + 3g_A^2)/(16m_e^2)$ and $\kappa_p = \sigma_0[4\sin^4\theta_W - 2\sin^2\theta_W + (1 + 3g_A^2)/4]/(4m_e^2)$, where $\sin^2\theta_W \simeq 0.231$ and $g_A \simeq -1.26$ is the axial-vector coupling constant. The characteristic length-scale of neutrino absorption l_ν is difficult to calculate directly due to the complex and dynamic structure of solutions. Instead we use the following simplification $l_\nu = \frac{\rho}{\sqrt{\rho}} \approx \left(0.27 + 1.5\frac{\rho}{10^{12}}\right) r_g$, where $r_g = GM_{BH}/c^2$ is the gravitational radius of BH.

At very high densities $\rho > 8.1 \times 10^6$ g cm⁻³ the process of electron capture on nuclei becomes important. In order to take this into account we have utilised the results obtained in [26] and made a simple approximation which is 7% accurate.

SIMULATION SETUP

The simulations are carried out with an upwind conservative scheme that based on a linear Riemann solver and uses the constrained transport method to evolve magnetic field. The details of this numerical method and various tests are described in [29, 30]. The neutrino cooling is introduced via the source term in the energy-momentum equation

$$\partial_\nu(\sqrt{-g}T_\mu^\nu) = \sqrt{-g}Su_\mu,$$

where u^ν is the four-velocity of plasma, g is the determinant of metric tensor, and S is the cooling rate as measured in the fluid frame. The gravitational attraction of BH is introduced via the Kerr metric in Kerr-Schild coordinates, $\{t, \phi, r, \theta\}$. The two-dimensional computational domain is $(r_0 < r < r_1) \times (0 < \theta < \pi)$, where $r_0 = (1 + \sqrt{1 - a^2}/2) r_g$, there $r_g = 14.847$ km and $r_1 = 200 r_g = 2969$ km. The total mass within the domain is small compared to the mass of BH (less than 25%) that allows us to ignore its self-gravity. The grid is uniform in θ where it has 320 cells and almost uniform in $\log(r)$ where it has 459 cells, the linear cell size being the same in both directions.

The initial solution describes an equilibrium torus with constant specific angular momentum l_0 [31, 32]. The black hole mass $M_{BH} = 10M_\odot$ and its rotation parameter $a = 0.9$. The torus mass $M_{tor} = 2.55M_\odot$ and its specific angular momentum $l_0 = 2.8r_g c = 1.25 \times 10^{17} \text{ g cm}^2 \text{ sec}^{-1}$. This setup corresponds to the collapse of a massive star when its core and inner envelope form a black hole and the outer envelope forms an accretion disk. The initial magnetic field is purely poloidal, thus the only non-zero component of its vector potential is $A_\phi \propto W(r, \theta)^3$, here $W(r, \theta) = \frac{1}{2} \ln \left| \frac{g_{t\phi}g_{t\phi} - g_{tt}g_{\phi\phi}}{g_{\phi\phi} + 2l_0g_{t\phi} + l_0^2g_{tt}} \right|$. The ratio of magnetic to gas pressure $\beta = P_m/P_g$ does not exceed 3×10^{-2} . In the initial solution more than 80% of the total pressure comes from the radiation and only 20% from the degenerated matter. In these conditions the neutrino cooling is important.

RESULTS

After initial period of relaxation all our models show the same structure involving a thick disk, a highly magnetised jet and a wind from the disk. The fast neutrino cooling in the optically thin model DL2A9C leads to significant imbalance of the torus. The torus collapses to a new state where its thermal pressure becomes negligible. In the model DL2A9MC, where we take into account the opacity effects, the torus interior is optically thick to neutrinos. This model develops a slightly different structure where the halo is squeezed as in model DL2A9MC but the central core is bigger and has a higher temperature ($T \approx 2.2 \times 10^{11}$ K) compared to the model DL2A9C. Figure 1 shows the impact of neutrino cooling on the structure of the torus. Without cooling the torus keeps the same size and shape as in the initial solution. The strong cooling in model DL2A9C leads to the collapse of initial configuration with the peak density increasing 10-fold and reaching $10^{13} \text{ g cm}^{-3}$. The moderate cooling in model DL2A9MC results in lower peak density, $3 \times 10^{12} \text{ g cm}^{-3}$. In DL2A9MC and DL2A9C the accretion flow is thinner than in DL2A9NC (see fig.1). In DL2A9NC the highly magnetised jet region is much smaller and more variable than in DL2A9C and DL2A9MC. However, the global structure of the accretion flow does not change very much and the energy release rate in jets of all models is similar. In model DL2A9MC the efficiency,

$$\eta = \int_0^T \dot{E}_{tor} dt / \int_0^T \dot{M}_{BH} c^2 dt,$$

is about 0.003. In model DL2A9NC it is 3.8 times lower.

At the start of simulations the central regions of models with cooling loose pressure support and begin to fall into the potential well. This leads to the oscillations similar to

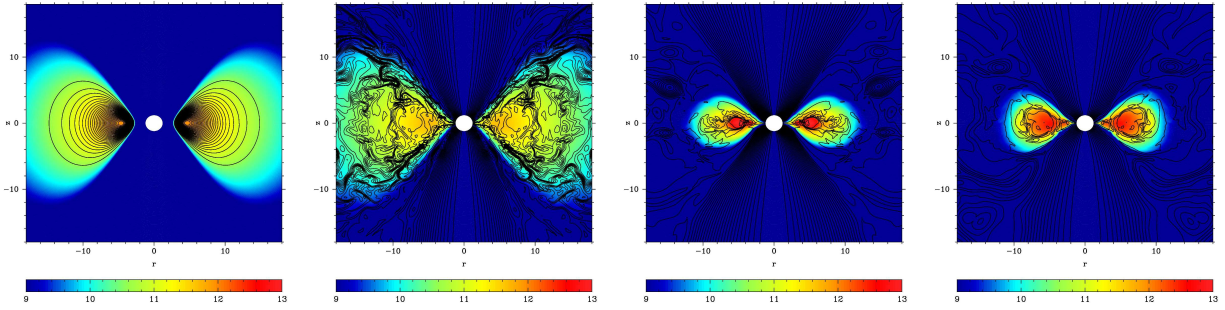


FIGURE 1. $\log_{10}(\rho)$ (colour image) and magnetic field lines. The initial solution for all models is shown in the upper left panel. The other panels from left to right show solutions after 0.2075 sec; model DL2A9NC (second on the left), model DL2A9C (second on the right), model DL2A9MC (first on the right).

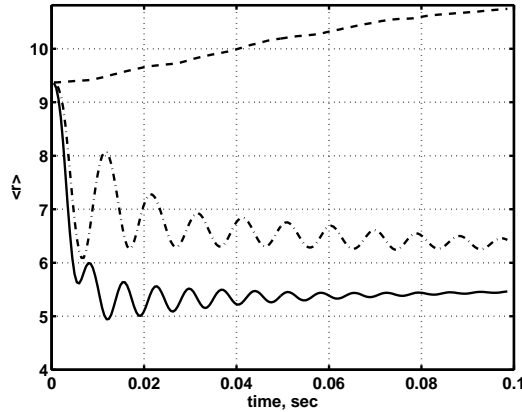


FIGURE 2. Evolution of the mass-averaged torus radius. Dashed line – DL2A9NC, dot-dashed – DL2A9MC, solid – DL2A9C.

those reported in [33]. However, we observe fast dumping of these oscillations (see fig. 2) One reason is the strong radiative shocks driven into the outer layers of the torus which are slow to react to the loss of equilibrium. The other reason is Maxwell stresses. In the optically thin case (model DL2A9C) the initial amplitude of oscillations $dr^m/r^m = 0.05$, where $r^m = \int_M r dm / \int_M dm$ is the mass-averaged torus radius. The oscillations degrade quickly with the quality factor $Q = |(dr_i^m + dr_{i+1}^m)/2(dr_i^m - dr_{i+1}^m)| = 3.8$, here dr_i^m is maximal deviation from equilibrium of i -th oscillation. The estimated relaxation time is $t_{relax} = t_{osc} \times Q \approx 0.027$ sec. In model DL2A9MC with less effective cooling the initial amplitude of oscillations is higher, $dr^m/r^m = 0.15$, but the quality factor is lower, $Q = 1.6$. After few oscillations the amplitude decreases to $dr^m/r^m = 0.05$, the effective viscosity decreases and the quality factor grows to $Q = 6.7$. The corresponding relaxation time $t_{relax} \approx 0.063$ sec. When neutrino cooling is not included the oscillations do not appear at all and the mass-averaged radius of the torus increases in time due to the development of wind.

TABLE 1. Main results.

model	l	a	\dot{M}_{BH}	\dot{M}_w	E_{51}^{tot}	η
DL2A9NC	2.8	0.9	1.3937	0.0189	1.8530	0.00074
DL2A9C	2.8	0.9	0.8588	0.0134	2.9039	0.0019
DL2A9MC	2.8	0.9	0.512	0.0276	2.577	0.0028

DISCUSSION AND CONCLUSIONS

In all our models we observe the development of a Poynting-dominated jet from BH. The neutrino cooling processes do not have a significant effect on the jet power. In fact it appears to be less disrupted due to interactions with disk wind and corona. On the other hand, the disk wind weakens when the cooling is included. The estimated total energy release during the whole period of accretion $E_{tot} \approx \eta M_{torus} c^2 \sim 10^{52}$ erg. This can explain the energetics of hypernovae explosions associated with GRB 980425 and GRB 030329. The studies of magnetic acceleration of Poynting-dominated jets show that high terminal Lorentz factors can be achieved together with effective conversion of electromagnetic energy into the bulk motion energy of the jet [34, 35]. Thus, this is a promising model of central engines of Gamma Ray Bursts.

Our model is complimentary to the model of magnetar driven GRBs and hypernovae, e.g. [36]. Both these models explain the origin of collimated GRB jets and power of hypernovae. Further investigation is required to distinguish these two scenario and determine their specific observational signatures. At the moment we can only say that the chemical composition of the jet will differ. In the collapsar case we expect highly Poynting dominated e^+e^- jets from onset whereas in the magnetar model the jets are initially strongly contaminated by baryons.

The disc oscillations observed in our simulations are the product of initial setup because the effects of neutrino cooling have not been included in the initial equilibrium solution. They are quickly dumped and thus unlikely to be excited in realistic astrophysical conditions. This conclusion is supported by the simulations where the formation of accretion disks is followed from the onset of stellar collapse [12, 13].

ACKNOWLEDGMENTS

The author would like to thank S.S. Komissarov and G.S.Bisnovatyi-Kogan for help in calculations and discussions. This calculations were carried out on St Andrews UK MHD cluster and the White Rose Grid facilities. This research is funded by PPARC/STFC under the rolling grant ‘‘Theoretical Astrophysics in Leeds’’.

REFERENCES

1. Bloom J.S., Kulkarni S.R., Djorgovski S.G., *Astronomical Journal* **123**, 1111–1148 (2002)
2. Fruchter A.S., Levan A.J., Strogler L., Vreeswijk P.M., et al., *Nature* **441**, 7092, 463–468 (2006)
3. Blinnikov S.I., Postnov K.A., Kosenko D.I., Bartunov O.S., *Astron. Lett.* **31**, 6, 365–374 (2005)

4. Soffitta P., Feroci M., Piro L., Zand J., Heise J. et al., *IAU Circ* **6884**, 1 (1998)
5. Galama T.J., Vreeswijk P.M., van Paradijs J. et al., *Nature* **395**, 6703, 670–672 (1998)
6. Pian E., Amati L., Antonelli L.A., Butler R.C. et al., *Astrophysical Journal* **536**, 778–787 (2000)
7. Greiner J., Peimbert M., Estaban C. et al., *GCN* **2020**, (2003)
8. Matheson T., Garnavich P.M., Stanek K.Z. et al., *Astrophysical Journal* **599**, 394–407 (2003)
9. Hjorth J., Sollerman J., Møller P., Fynbo J.P.U. et al., *Nature* **423**, 6942, 847–850 (2003)
10. Sokolov V.V., Fatkhullin T.A., Komarova V.N. et al., *Bull. Spec. Astroph. Obser.* **56**, 5–14 (2003)
11. Woosley S.E., *Astrophysical Journal* **405**, 273–277 (1993)
12. MacFadyen A.I. & Woosley S.E., *Astrophysical Journal* **524**, 262–289 (1999)
13. Barkov M.V., Komissarov S.S., *Month. Not. Royal Astron. Soc.: Lett.* **385**, L28–L32 (2008)
14. De Villiers J.P., Hawley J.F., Krolik J.H., *Astrophysical Journal* **599**, 1238–1253 (2003)
15. Hawley J.F., Krolik J.H., *Astrophysical Journal* **641**, 103–116 (2006)
16. McKinney J.C., Gammie C.F., *Astrophysical Journal* **611**, 977–995 (2004)
17. McKinney J.C., *Month. Not. Royal Astron. Soc.* **368**, 1561–1582 (2006)
18. Blandford R.D. & Znajek R.L., *Month. Not. Royal Astron. Soc.* **179**, 433–456 (1977)
19. Shibata M., Sekiguchi Yu, Takahashi R., *Progress of Theor. Physics* **118**, 2, 257–302 (2007)
20. Ardeljan N.V., Bisnovatyj-Kogan G.S., et al., *Month. Not. Royal Astron. Soc.* **359**, 333–344 (2005)
21. Schinder P. J., Schramm D. N., Wiita P. J., et al., *Astrophysical Journal* **313**, 531–542 (1987)
22. Ivanova L.N., Imshennik V.S., Nadezhin D.K., *Nauchnye Informatsii* **13**, 3 (1969)
23. Bezchastnov V.G., Haensel P., et al., *Astronomy and Astrophysics* **328**, 409–418 (1997)
24. Thompson T.A., Burrows A., Meyer B.S., *Astrophysical Journal* **562**, 887–908 (2001)
25. Tubbs D.L., Schramm D.N., *Astrophysical Journal* **201**, 467–488 (1975)
26. Baym G., Pethick Ch., Sutherland P., *Astrophysical Journal* **170**, 299–306 (1971)
27. Nagataki S., Takahashi R., Mizuta A., Takiwaki T., *Astrophysical Journal* **659**, 512–529 (2007)
28. Birkl R., Aloy M.A., Janka H.Th., Müller E., *Astronomy and Astrophysics* **463**, 51–67 (2007)
29. Komissarov S.S., *Month. Not. Royal Astron. Soc.* **303**, 343–366 (1999)
30. Komissarov S.S., *Month. Not. Royal Astron. Soc.* **350**, 1431–1436 (2004)
31. Fishbone L.G., Moncrief V., *Astrophysical Journal* **207**, 962–976 (1976)
32. Abramowicz M., Jaroszynski M., Sikora M., *Astronomy and Astrophysics* **63**, 221–224 (1978)
33. Zanutti O., Font J.A., Rezzolla L., Montero P.J., *Month. Not. Royal Astron. Soc.* **356**, 1371–1382 (2005)
34. Komissarov S.S., Barkov M.V., Vlahakis N., Königl A., *Month. Not. Royal Astron. Soc.* **380**, 51–70 (2007)
35. Barkov M.V., Komissarov S.S., *preprint: astro-ph* **0801.4861**, 1–4 (2008)
36. Komissarov S.S., Barkov M.V., *Month. Not. Royal Astron. Soc.* **382**, 1029–1040 (2007)